ACS APPLIED MATERIALS & INTERFACES

www.acsami.org Research Article

Enzyme Nanoreactor for *In Vivo* Detoxification of Organophosphates

Tatiana Pashirova, Zukhra Shaihutdinova, Milana Mansurova, Renata Kazakova, Dinara Shambazova, Andrei Bogdanov, Dmitry Tatarinov, David Daudé, Pauline Jacquet, Eric Chabrière, and Patrick Masson*

Cite This: https://doi.org/10.1021/acsami.2c03210 Read Online

ACCESS | Metrics & More | Article Recommendations | Supporting Information

ABSTRACT: A nanoreactor containing an evolved mutant of *Saccharolobus solfataricus* phosphotriesterase (L72C/Y97F/Y99F/W263V/I280T) as a catalytic bioscavenger was made for detoxification of organophosphates. This nanoreactor intended for treatment of organophosphate poisoning was studied against paraoxon (POX). Nanoreactors were low polydispersity polymersomes containing a high concentration of enzyme (20 μM). The polyethylene glycol−polypropylene sulfide membrane allowed for penetration of POX and exit of hydrolysis products. *In vitro* simulations under second order conditions showed that 1 μM enzyme inactivates 5 μM POX in less than 10 s. LD_{50}-shift experiments of POX-challenged mice through intraperitoneal (*i.p.*) and subcutaneous (*s.c.*) injections showed that intravenous administration of nanoreactors (1.6 nmol enzyme) protected against 7 × LD_{50} *i.p.* in prophylaxis and 3.3 × LD_{50} *i.p.* in post-exposure treatment. For mice *s.c.*-challenged, LD_{50} shifts were more pronounced: 16.6 × LD_{50} in prophylaxis and 9.8 × LD_{50} in post-exposure treatment. Rotarod tests showed that transitory impaired neuromuscular functions of challenged mice were restored the day of experiments. No deterioration was observed in the following days and weeks. The high therapeutic index provided by prophylactic administration of enzyme nanoreactors suggests that no other drugs are needed for protection against acute POX toxicity. For post-exposure treatment, co-administration of classical drugs would certainly have beneficial effects against transient incapacitation.

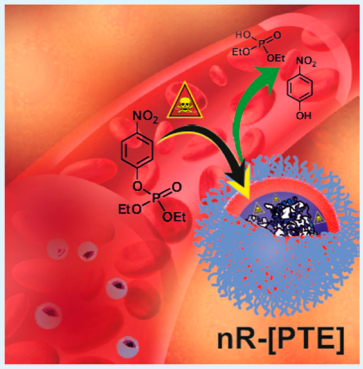

KEYWORDS: *nanoreactor, organophosphate poisoning, paraoxon, phosphotriesterase, post-exposure treatment, prophylaxis, polymersomes*

1. INTRODUCTION

Though the use of organophosphate (OP) pesticides is decreasing, these compounds still represent a serious threat for populations all over the world. More than 100,000 people annually die of accidental or intentional poisoning by OP pesticides.[1] Moreover, synthesis of these compounds is easy. Thus, OP pesticides or banned chemical warfare agents could potentially be used in terrorist acts or for assassination.[2] Irreversible inhibition of acetylcholinesterase (AChE) due to fast phosphylation of the enzyme active site is responsible for the acute toxicity of OPs.[3] Prophylaxis and emergency treatments of OP poisoning by using pharmacological drugs are still imperfect.[4] However, the concomitant developments of nanotherapies and bioscavengers have opened new perspectives. Nanodetoxification strategies to develop antidotal nanoparticles specifically for detoxification emerged recently.[5−8] Nanoparticles containing enzymes or chemicals with high affinity, selectivity and high reactivity toward various toxic molecules are actively expanding.[9−12] In the past years, nanomedicine solutions were introduced in the therapeutic arsenal against OP toxicity. We previously proposed oxime-loaded nanoparticles for emergency treatment of OP poisoning.[13−16] At the same time, the use of injectable enzymes (bioscavengers) capable of neutralizing OP molecules in the bloodstream appeared as an alternative to classical pre- and post-exposure treatments.[4] The most potent OP-degrading enzymes to be used as catalytic bioscavengers are evolved bacterial phosphotriesterases (PTE).[17,18] Attempts to use OP-hydrolyzing enzymes, for protection against OP poisoning, have been made for years. Administered OP-hydrolyzing enzymes can be either free enzymes[19−21] or encapsulated enzymes into liposomes or other nanoparticles.[22−24] In most reported works, enzyme administration was associated with classical therapeutic drugs like atropine and oximes. However, to prevent host immune response and increase the time life of administered enzymes, nonhuman enzymes must be encapsulated in sealed nanocontainers. Thus, PTE-catalyzed hydrolysis of OPs takes place in the nanocontainer body, where the enzyme concentration is much higher than that of the OP that diffuses into the nanoreactor from the blood.[24] Unlike liposomes, nanoreactors—for encapsulated enzymes—are

Received: February 21, 2022
Accepted: April 7, 2022

highly stable sealed spherical nanoparticles of diameter of the order of 100 nm with a permeable polymeric membrane. Diblock and triblock copolymer amphiphiles can form lyotropic lamellar mesophases and vesicular structures similar to phospholipids and a membrane-forming amphiphiles.[25−27] As a result, a new class of synthetic containers with a shell based on *block* copolymers can be formed, providing improved properties and features, in particular, a high chemical versatility[25,28,29] compared to liposomes. The structural features and properties of polymersomes, including stability, fluidity, and intermembrane dynamics, are highly dependent on *block* copolymer characteristics.[30,31] In contrast to liposome containers, polymer vesicles are more applicable to accommodate large hydrophilic macromolecules like enzymes.[32−34] Several polymer nanopharmaceuticals have been approved for clinical use.[35] However, clinical uses are often limited by the low biodegradability of polymeric carriers. Therefore, it is necessary to design effective nanodetoxicants based on nonirritating and biodegradable nanomaterials. The most promising and expectedly inspiring are polyethylene glycol (PEG)-containing and stimuli-responsive polymers.[36] Thus, PEG−polypropylene sulfide (PPS) scaffolds are biocompatible[37] and applicable for different biomedical purposes,[38−42] in particular of potential interest for therapeutic uses in humans.[43] In addition, PEG−PPS nanocarriers can be scalably produced.[44]

In the nanoreactor approach we are developing, PTE-catalyzed detoxification reaction takes place inside the nanoreactor body (Figure 1) where the enzyme concentration

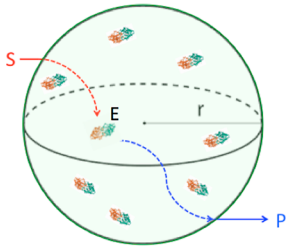

Figure 1. Scheme of the enzyme-containing nanoreactor ($r \approx 50-75$ nm) for hydrolytic detoxification of OPs. OP substrate, S = OP; P = nontoxic hydrolysis products. The encapsulated enzyme (E) is a dimeric *Saccharolobus solfataricus*PTE mutant (72 kDa). PTE-catalyzed hydrolysis of OP takes place in the nanoreactor core where OP and P enter and exit freely by simple diffusion across the nanoreactor membrane.

is high, far higher than OP concentration in blood, encountered in the most severe cases of poisoning. Thus, the detoxification reaction is second-order.[24]

In the present work, we investigated the therapeutic action in mice of injected *Saccharolobus solfataricus* PTE mutant-containing nanoreactors against the acute toxicity of paraoxon (POX) as a model OP. POX is the active metabolite of the pesticide parathion after cytochrome P450 activation in the liver. POX as other OPs is a potent phosphorylating agent of AChE. The bimolecular reaction constant of human AChE with POX, $k_i = 7 \times 10^5$ M^{-1} min^{-1}.[45]

2. MATERIALS AND METHODS

2.1. Chemicals. POX-ethyl (POX, purity ≥ 90%, Sigma-Aldrich, product of Canada), *p*-nitrophenol (pNp, 99%, Alfa Aesar, Karlsruhe, Germany), rhodamine B (99%, ACROS Organics, NJ, USA), poly(ethylene glycol) methyl ether, average M_n = 750 (mPEG, Sigma-Aldrich, USA), propylene sulfide (stabilized with Butyl Mercaptan) (PS, Tokyo Chemical Industry Co., Ltd, Tokyo, Japan), and potassium thioacetate (98%, Sigma-Aldrich, Switzerland) were used. All other chemicals and solvents were of chemical or biochemical grade. Ultrapurified water (18.2 MΩ cm resistivity at 25 °C) was produced from Direct-Q 5 UV equipment (Millipore S.A.S. 67120 Molsheim, France).

2.2. Enzyme. A previously engineered evolved mutant of SsoPox, a phosphotriesterase-like lactonase (PLL) of 72 kDa from the hyperthermophilic archaea *Saccharolobus solfataricus*, was considered to prepare enzymatic nanoreactors. This variant, referred to as SsoPox-IIIC1, carries five mutations compared to the wild-type enzyme (L72C/Y97F/Y99F/W263V/I280T). SsoPox-IIIC1 was shown to have a drastically enhanced phosphotriesterase activity toward POX with a k_{cat}/K_m value of 1.1×10^5 M^{-1} s^{-1} at 25 °C.[18] The enzyme displays michaelian behavior with OPs as substrates. This dimeric enzyme of 35 kDa/monomer also shows a high thermostability (T_m = 96.3 °C), ensuring easy handling, compatibility to encapsulation methods, and long-term stability.[46,47] SsoPox-IIIC1 was expressed in BL21(DE3)-containing pGro7 plasmid (TaKaRa) and purified, using size exclusion chromatography, to homogeneity as described previously.[48] Briefly, BL21(DE3) cells containing chaperones and SsoPox-IIIC1 plasmids were grown in ZYP medium (complemented with chloramphenicol 34 μg/mL and ampicillin 100 μg/mL) at 37 °C. When an OD600 nm around 0.8−1 was reached, induction was realized by decreasing the temperature to 23 °C and adding 0.2% L-arabinose and 0.2 mM $CoCl_2$. After 20 h of growth, cells were harvested by centrifugation (4400 g, 20 min at 15 °C) and pellets were resuspended in 50 mM HEPES buffer pH 8.0, containing 150 mM NaCl, 0.25 mg/mL lysozyme, 0.1 mM PMSF, and 10 μg/mL DNAseI. Following an overnight storage at −80 °C, cells were sonicated (3 × 30 s in Qsonica, Q700; amplitude 45), heated at 70 °C for 30 min, and then centrifuged (15 min at 10,000 g) to eliminate cellular debris and nonthermostable proteins. Ammonium sulfate (75%) precipitation was realized with supernatants, overnight at 4 °C, to concentrate proteins before purification. Finally, two steps of purification were performed, using a desalting column (HiPrep 26/10 desalting, GE Healthcare; ÄKTA Avant), and gel filtration (HiLoad 16/600 SuperdexTM 75 pg, GE Healthcare; ÄKTA Avant) in 50 mM HEPES pH 8.0 buffer, containing 150 mM NaCl. The enzyme purity (88%) was verified by electrophoresis in denaturing conditions sodium dodecyl sulfate−poly acrylamide gel electrophoresis (SDS−PAGE), T = 12.5% acrylamide) (Figure 2), enzyme concentration was determined using a NanoDrop 2000 spectrophotometer (Thermo Scientific), and enzyme activity toward POX was measured in a microplate reader (Synergy HT, BioTek, USA) at 25 °C in 50 mM HEPES pH 8.0 buffer, containing 150 mM NaCl. Then, the enzyme preparation was lyophilized.

Left lane, molecular weight markers; right lane, highly purified SsoPox-IIIC1 (quintuple mutant L72C/Y97F/Y99F/W263V/I280T), monomer of 36 kDa. The impurity of 70 kDa corresponds to the co-expressed chaperon protein.

2.3. Catalytic Activity of the Enzyme Preparation. The enzyme activity was currently determined under standard conditions, at 25 °C, in 10 mM Tris buffer, pH 7.4, supplemented with 0.2 mM $CoCl_2$. POX stock solutions (100; 10 and 1 mM) were in ethanol (EtOH). However, because the enzyme was administered to animals and thus was operational *in vivo* at 37 °C, catalytic parameters were also determined at 37 °C. For determination of catalytic parameters, POX concentration ranged from 5 to 1250 μM; the final EtOH in the cuvette was 1.5%. Steady-state kinetics was recorded by monitoring the release of pNp at 400 nm for 180 s. The molar extinction coefficient of pNp is 11,554 M^{-1} cm^{-1} at pH = 7.4. The final enzyme concentration per assay was 0.01 μM. Measurements were performed in triplicates. The catalytic parameters K_m, k_{cat}, and k_{cat}/K_m were determined by nonlinear fitting of the Michaelis−Menten equation using Origin software (OriginLab Co, Northampton, MA, USA).

2.4. Animals. Male CD-1 mice (weighing 18−22 g) were purchased from the "Biotech Scientific and Production Complex"

https://doi.org/10.1021/acsami.2c03210
ACS Appl. Mater. Interfaces XXXX, XXX, XXX−XXX

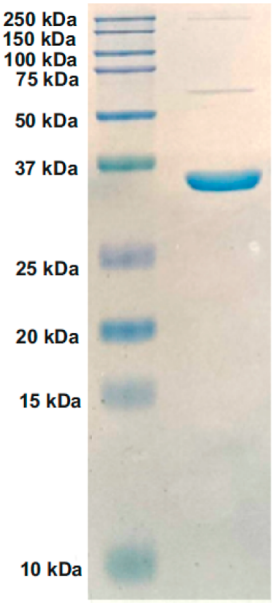

Figure 2. SDS−PAGE of SsoPox-IIIC1.

LLC, Russia. All animals were acclimatized for 2 weeks before experiments. They were housed in sawdust-lined polypropylene cages, maintained under standard conditions (12 h light/dark cycle; 22 ± 3 °C and a 50 ± 20% relative humidity). Animals were given standard pellet diet and water ad libitum throughout the course of the study. All experimental procedures with animals were performed in accordance with the Ethical Principles in Animal Research and were approved by the Local Ethics Committee of the Kazan Federal University (protocol no 33).

2.5. Synthesis of Nanoreactor Polymeric Envelopes. Polymeric envelopes of nanoreactors were made of altered *block* unit, PEG−PPS, type. Synthesized copolymers are noted $A_mB_nA_m$, where A represents the PEG domain, B is the PPS domain, and m and n are the number of repeating units in respective polymer chains. Rational for choosing PEG and PPS, and interest of these polymers for making nanoreactor envelopes are developed in the Supporting Information file (SI).

2.6. Analytical Controls of Polymer Structures. ^{1}H and ^{13}C NMR spectra were recorded on 400 MHz [400.1 MHz (^{1}H), 100.6 MHz (^{13}C)] or 600 MHz [600.1 MHz (^{1}H), 150.9 MHz (^{13}C)]. Chemical shifts are reported on the δ (ppm) scale and are relative to the residual ^{1}H and ^{13}C signal of $CDCl_3$, and all coupling constant (J) values are given in Hz. ^{1}H NMR and ^{13}C spectra for all compounds are in the Supporting Information file (Figures S1−S4). Infrared (IR) spectra of synthesized molecules were recorded on a Bruker Tensor-27 instrument for samples in KBr pellets. IR spectra are in the Supporting Information file (Figures S5−S7).

2.7. Poly(ethylene glycol) Methyl Ether Tosylate (mPEGTs-750) (2). (2) was synthesized according to the reported procedure[49] in toluene using Et_3N as a base. A solution of 3 g (4 mmol) of mPEG-750 in toluene was dried by azeotropic distillation with toluene, using Dean−Stark trap and cooled to room temperature. Then, 2.7 mL (2.02 g, 20 mmol) of Et_3N was added, followed by 1.53 g (8 mmol) of *p*-toluene sulphonyl chloride. The solution was stirred overnight at room temperature, and the formed triethylammonium hydrochloride was filtered. Toluene and all volatile components were rotary-evaporated (bath temperature 40 °C). Light-brown oil was washed several times with diethyl ether and dried in vacuum to give mPEGTs-750 (2) as a light-brown paste. (3.24 g, 90%), ^{1}H NMR (600 MHz, $CDCl_3$) δ: 7.81 [d, J = 8.2 Hz, 2H, CH(Tol)], 7.35 (d, J = 8.0 Hz, 2H, CH(Tol)), 4.17 (t, J = 4.8 Hz, 2H, O−$CH_2\underline{CH_2}OSO_2$−), 3.71−3.68 (m, 2H, O−$\underline{CH_2}CH_2OSO_2$−), 3.68−3.63 (m, 73H, CH_2, broad, PEG chain protons), 3.39 (s, 3H, CH_3O), 2.46 [s, 3H, CH_3(Tol)]. FT-IR 3478, 2873, 1466, 1354 (ν_{as} SO_3), 1282, 1249, 1180 (SO_2), 1177 (ν_s SO_3), 1109, 1035, 1013, 924, 845, 819, 777, 681, 664, 555.

2.8. Poly(ethylene glycol) Methyl Ether Thioacetate (mPEGSAc-750) (3). (3) was synthesized according to the slightly modified previously reported procedure.[50] In a Schlenk tube, 0.9 g (∼1 mmol) of mPEGTs-750 (2) was evacuated in vacuum, flushed with argon three times, and dissolved in dry *N*,*N*-dimethylformamide (DMF) (30 mL) followed by the addition of potassium thioacetate (0.57 g, 5 mmol) in one portion. The mixture was stirred at room temperature overnight. DMF was removed on a rotary evaporator (bath temperature 40 °C). The oily residue was dissolved in DCM and stirred with activated charcoal for 1.5 h followed by filtration on the Schott funnel. The filtrate was rotary-evaporated and dissolved in diethyl ether. After a solution was left overnight, the white precipitate was filtered and the filtrate was evaporated and vacuum-dried to give mPEGSAc-750 (3) as a brown oil (0.81 g, 98%), ^{1}H NMR (600 MHz, $CDCl_3$, 30\degc) δ: 3.66 (s, 73H, CH_2 broad, PEG chain protons), 3.58−3.55 (m, 2H, −O$\underline{CH_2}CH_2S$−), 3.39 (s, 3H, CH_3O), 3.11 (t, J = 6.4 Hz, 2H, −$\underline{CH_2}SCOCH_3$), 2.37 (s, 3H, $CH_3C(O)S$). FT-IR 3505, 3458, 2887, 1690 (C═O), 1468, 1360, 1343, 1281, 1242, 1149, 1107, 1060, 963, 947, 842, 689, 624, 571, 529.

2.9. Poly(ethylene glycol)-*block*-poly(propylene sulfide)-*block*-poly(ethylene glycol) (mPEG−PPS−mPEG) (6). (6) was synthesized according to a procedure reported earlier.[51] In a Schlenk tube, 0.5 g (0.6 mmol) of mPEGSAc-750 (3) was evacuated in vacuum, flushed with argon three times, and then dissolved in freshly distilled tetrahydrofuran (THF) (20 mL). Sodium methoxide prepared by dissolving of 16 mg of sodium in 1.4 mL of absolute methanol under an argon atmosphere was added via a syringe, and the mixture was stirred at room temperature for 30 min. Then, 2 mL (1.89 g, 25.5 mmol) of propylene sulfide was added via a syringe and the mixture was stirred for 1 h, and then, the Schlenk tube was opened and the mixture was exposed to air overnight at room temperature. The solvents and all volatile components were removed in vacuum to give light-brown oil that was subsequently dissolved in 20 mL of DCM. A light-brown precipitate formed when the solution was left overnight. The precipitate was filtered and the filtrate was evaporated and vacuum-dried to give mPEG−PPS−mPEG (6) as a brown oil (1.79 g, 88%). ^{1}H NMR (600 MHz, $CDCl_3$, 30\degc) δ: 3.73 (q, J = 6.9 Hz, 4H, $\underline{CH_2}OCH_3$), 3.66 [br.s, 150H, CH_2 (PEG)], 3.58−3.55 (m, 4H, $OCH_2CH_2CH_2S$), 3.40 (s, 6H, OCH_3), 3.09−2.99 (m, 4H, CH_2SSCH_2), 2.99−2.86 [m, 134H, CH_2 (PPS)], 2.78−2.73 (m, 1H, CH_2S), 2.70 - 2.60 [m, 60H, CH (PPS)], 1.40 [br.s, 211H, CH_3 (PPS)]. ^{13}C NMR (101 MHz, $CDCl_3$, 30\degc) δ: 71.94 (s, CH_2OCH_3), 70.57 (s, J = 55.0 Hz, PEG-CH_2), 58.95 (s, CH_3O), 41.32 (s, CH-PPS), 41.27−41.21 (m, CH-PPS), 38.40 (s, CH_2-PPS), 20.74 (s, CH_3-PPS). FT-IR 3466, 2958, 2920, 2867, 1450, 1373, 1304, 1252, 1174, 1106, 1042, 1002, 650, 850, 734, 688, 571.

2.10. Preparation of mPEG−PPS−mPEG Polymersomes. mPEG−PPS−mPEG (0.5−5 % wt/wt) was dissolved in 1 mL of ethanol/chloroform (1:1). The homogeneous solution was kept in a water bath at 60 °C until alcohol evaporation. 10 mM Tris-buffer (pH 7.4) was preheated to 37 °C and added to rehydrate the copolymer at 37 °C in the absence or presence of PTE (0.02 mM), pNp (0.1 % wt/wt). The solution was stirred under magnetic stirring (750 rpm) (Heidolph, Germany) for 1 h at the same temperature (37 °C) and then within 24 h at 25 °C.

2.11. Characterization of mPEG−PPS−mPEG Polymersomes. The mean particle size, zeta potential, and polydispersity index (PDI) were determined by dynamic light scattering (DLS), using a Malvern Instrument Zetasizer Nano (Worcestershire, UK) and Litesizer 500 Anton Paar (Anto Paar GmbH, Austria). The size (hydrodynamic diameter, nm) was calculated according to the Einstein−Stokes relationship $D = k_BT/3\pi\eta x$, in which D is the diffusion coefficient, k_B is the Boltzmann's constant, T is the absolute temperature, η is the viscosity, and x is the average hydrodynamic diameter of nanoparticles. The diffusion coefficient was determined at least in triplicate for each sample. The average error of measurements was approximately 10%. All samples were analyzed in triplicate.

https://doi.org/10.1021/acsami.2c03210
ACS Appl. Mater. Interfaces XXXX, XXX, XXX−XXX

Transmission electron microscopy (TEM) was used to image the size and to reveal the morphology of both empty and PTE-loaded polymersomes. TEM images were obtained, using a Hitachi HT7700 Exalens microscope, Japan. The images were acquired at an accelerating voltage of 100 keV. Samples (mPEG−PPS−mPEG, 20 μg/mL) were added to a 300 mesh copper grids with continuous carbonformvar support films.

Nanoparticle tracking analysis (NTA) was used to visualize and measure particle size and concentration. The total concentration (particles/mL) was obtained using NanoSight LM10 (Malvern Panalytical, Worcestershire, UK). Samples containing higher numbers of particles were diluted in 10 mM Tris buffer pH 7.4 (mPEG−PPS−mPEG, 0.4 μg/mL) before analysis, and the relative concentration was then calculated according to the dilution factor. These dispersions were then injected into the measurement chamber of the instrument at room temperature using a syringe pump. The measurements were carried out in a special cuvette for aqueous solutions, equipped with a laser having a wavelength of 405 nm (CD version S/N 2990491), and the O-ring is made of the Kalrez material. A CMOS camera C11440-50B with an image capture sensor FL-280 Hamamatsu Photonics (Japan) was used as a detector. Temperature in the chamber was determined using a contact thermometer OMEGA HH804 (Engineering Inc.) for all measurements. The samples were measured for 60 s.

2.12. Encapsulation Efficiency (EE, %) and Loading Capacity (LC, %). Encapsulation efficiency (EE) (%) and loading capacity (LC) (%) were assessed for samples containing PTE (0.02 mM) and pNp (7.2 mM). These parameters were determined indirectly by filtration/centrifugation, measuring free PTE and pNp (nonencapsulated) by spectrophotometry.

A volume 400 μL of each PTE-loaded polymersomes was placed in centrifugal filter devices Milippore (100 kDa) to separate copolymer and aqueous phases and centrifuged at 3000 rpm for 3 min, using centrifuge Rotanta 460 (Hettich Zentrifugen, Germany). Concentration of free PTE was quantified by UV absorbance using PerkinElmer λ_{35} (PerkinElmer Instruments, USA) at 277 nm (ε = 15316 M^{-1} cm^{-1} in 10 mM Tris buffer pH = 7.4). The UV absorbance spectra and calibration curve are presented in Supporting Information file (Figure S8).

A volume of 100 μL of each pNp-loaded polymersomes was placed in centrifugal filter devices Nanosep centrifugal device 3K Omega (Pall Corporation) to separate copolymer and aqueous phases and centrifuged at 10,000 rpm for 15 min using centrifuge MiniSpin plus (Eppendorf AG, Hamburg, Germany). Free pNp was quantified by UV absorbance using PerkinElmer λ_{35} (PerkinElmer Instruments, USA) at 400 nm (ε = 11554 M^{-1} cm^{-1} in 10 mM Tris buffer pH = 7.4). The UV absorbance spectra and calibration curve are presented in Supporting Information file (Figure S9).

The encapsulation parameters, EE % and LC %, were calculated against the appropriate calibration curve using the following equations

$$\mathrm{EE}(\%) = \frac{\text{total amount of enzyme} - \text{free enzyme}}{\text{total amount of enzyme}} \times 100\% \quad (1)$$

$$\mathrm{LC}(\%) = \frac{\text{total amount of enzyme} - \text{free enzyme}}{\text{total amount of copolymer}} \times 100\% \quad (2)$$

2.13. Stability of Nanoreactors. 100 μL (empty and PTE-loaded nanoreactors, 10 mg/mL) was added to 0.9 mL different media (human plasma, 10 mM Tris buffer at pH 7.4) and incubated for 2 h at 37 °C. The size, zeta-potential, and PDI of nanoreactors were measured along time by DLS, using a Malvern Instrument Zetasizer Nano (Worcestershire, UK).

2.14. Purification of PTE-loaded Nanoreactors. To remove unencapsulated free enzymes from PTE-loaded polymersomes, we separated the two enzyme fractions by filtration/centrifugation using centrifugal filter devices Milippore (cut off = 100 kDa). Fractions of 1 mL were centrifuged at 3000 rpm for 3 min, using centrifuge Rotanta 460 (Hettich Zentrifugen, Germany) and monitored with a UV spectrometer at 277 nm. These conditions were found by monitoring the transmittance of empty polymersomes under centrifugation conditions over time. Transmittance of polymersomes is presented in the Supporting Information file (Figure S10).

2.15. *In Vitro* Simulations of Enzyme Nanoreactor Conditions: Spectrophotometric Kinetics of POX Hydrolysis in Cuvette Using Free and Encapsulated Enzymes. Nanoreactor simulation of POX inactivation was performed under second-order conditions in 1 cm spectrophotometric cuvettes in 10 mM Tris buffer, pH 7.4 at 25 °C. Enzyme-catalyzed hydrolysis of POX was monitored by the absorbance increase at 400 nm due to the release of its leaving group, pNp: kinetics of neutralization of POX (1 and 5 μM) by stoichiometric concentrations of PTE (1 and 5 μM) was carried out either by adding the whole dose of POX in a single volume or by adding POX progressively up to the desired final concentration. The maximum POX concentration, 5 μM, was chosen because it is of the order of the maximum OP concentration determined in the human blood in the most severe cases of poisoning by POX or parathion.

2.16. Membrane Permeability to Substrate/Product (4-Nitrophenol Release) *in Vitro*. Monitoring of pNp release from polymersomes was performed using the dialysis bag diffusion method. Dialysis bags retain polymersomes and allow the released pNp to diffuse into the medium. The bags were soaked in Milli-Q water for 12 h before use. 1 mL polymersomes were poured into the dialysis bag. The two bag ends were sealed with clamps. The bags were then placed in a vessel containing 100 mL of 10 mM Tris buffer pH 7.4, the receiving phase. The vessel was placed in a thermostatic shaker (New Brunswick, USA) at 37 °C, under a stirring rate of 150 rpm. At predetermined time intervals, 0.5 mL samples were withdrawn, and their absorbance at 400 nm was measured using a PerkinElmer λ_{35} spectrophotometer (PerkinElmer Instruments, USA). All samples were analyzed in triplicate.

2.17. POX LD_{50}-Shift in Mice (Pre- and Post-Exposure Treatments). Mice were stratified by weight and randomly assigned into groups of three or six per group. POX was extemporaneously diluted in hydroalcoholic isotonic saline solution (EtOH 10% in sodium chloride 0.9%). The final EtOH concentration per dose was 1 mg/kg. POX LD_{50} were determined by intraperitoneal (*i.p.*) and subcutaneous (*s.c.*) injections at POX doses ranging from 1 to 2 mg/kg. Injections of 0.2 mL POX solution per 20 g animal were performed *i.p.* or *s.c.*, using an insulin syringe. Because POX was in a hydroalcoholic solution, the EtOH effect was checked in a control group. Then, LD_{50} determinations were performed after pre-treatment (prophylactic) and post-exposure (therapeutic) treatment of animals by PTE-loaded nanoreactor solution. A single dose (1.6 nmole of enzyme in 100 μL solution per 20 g animal) was injected in the tail vein, using the insulin syringe. In pre-treatment LD_{50}-shift experiments, the nanoreactor solution was administered by injection in tail vein 5 min before POX challenge. Prophylactic LD_{50} shift was determined using POX doses ranging from 5 to 15 mg/kg *i.p.* and from 15 to 25 mg/kg *s.c.* In post-exposure treatment trials, the enzyme-containing nanoreactor solution was injected 1 min after POX challenge at doses from 2 to 5 mg/kg *i.p.* and from 5 to 15 mg/kg *s.c.*

The initial POX doses were selected as the doses expected to produce mortality in some animals. Further groups of animals were dosed at higher or lower fixed doses, depending on mortality in challenged animal groups, until the study objective was achieved. For each dose, three animals were used to minimize the number of animals. If in a group of three animals, an unequivocal response was obtained (all animals died or survived), and then, we proceeded to the next dose.

All animals were observed individually for symptoms and mortality after dosing with special attention during the first 4 h and twice a day thereafter for 2 weeks. Poisoned animals that did not survive died in less than 24 h. Died animals were autopsied. LD_{50} was calculated by Probit analysis using IBM SPSS Statistics software.

2.18. Rotarod Performance Test of Mice. Mice were trained 1 week before the experiment. For this purpose, they were placed on the rotarod apparatus (Neurobotics, Russia), the trip switch was set, and

https://doi.org/10.1021/acsami.2c03210
ACS Appl. Mater. Interfaces XXXX, XXX, XXX−XXX

Scheme 1. Synthetic Route to *Block*-Copolymer mPEG−PPS−mPEG (6)

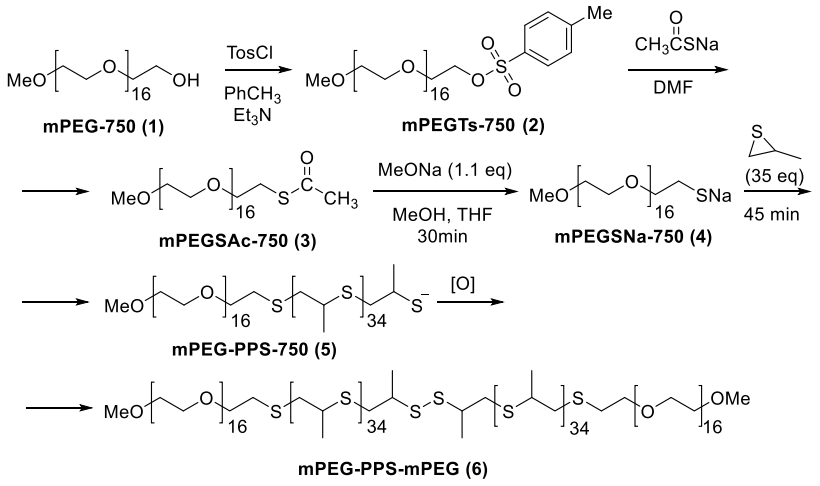

the beam was accelerated up to 30 rpm over 5 min. Mice were given three trials with at least 15 min of recovery time between each trial. If mice turned on the beam or felt down, they were replaced immediately.[52,53] Trained mice were randomly selected to form five groups (six animals per group).

Instead of POX- and PTE-loaded nanoreactors, equal volumes of saline solutions were *s.c.* and *i.v.* injected to the animals in the first control group. To perform pretreatment experiments, *i.v.* injection of saline solution was administered to three animals in this group, and after 5 min, saline solution was *s.c.* injected. To perform post-exposure treatment experiments, s.c. injection of saline solution was given to three other mice in this group, and then after 1 min, *i.v.* saline solution was administered.

Instead of POX and PTE-loaded nanoreactors, equal volumes of POX solvent (EtOH 10% in sodium chloride 0.9%, *s.c.*) and saline solution (*i.v.*) were administered to mice in the second solvent control group. To perform pretreatment experiments, *i.v.* injection of saline solution was administered to three animals in this group, and after 5 min, POX solvent was *s.c.* injected. To perform post-exposure treatment experiments, *s.c.* injection of POX solvent was given to three other mice in this group, and then, after 1 min, *i.v.* saline solution was administered.

Instead of POX and PTE-loaded nanoreactors, equal volumes of saline solution (*s.c.*) and empty polymersome solution (*i.v.*) were administered to mice in the third empty polymersome control group. To perform pretreatment experiments, *i.v.* injection of empty polymersome solution was administered to three animals in this group, and after 5 min, saline solution was *s.c.* injected. To perform post-exposure treatment experiments, *s.c.* injection of saline solution was given to three other mice in this group, and then, after 1 min, *i.v.* empty polymersome solution was administered.

PTE-loaded nanoreactors were injected (*i.v*), and 5 min later, POX at dose 11 mg/kg (i.e. pretreatment determined 1/2 LD_{50}) was *s.c.* injected to animals of the fourth group.

PTE-loaded nanoreactors (*i.v.*) were injected 1 min after challenge by POX (*s.c.*) at a dosage of 6.8 mg/kg (i.e., post-treatment determined 1/2 LD_{50}) to mice of the fifth group.

Animals were put on the beam immediately after injections and then after 1 and 2 h. The rotarod test was then performed under the same conditions as the training protocol. For each animal, the latency time to fall off the rod was noted. The rotarod test was carried out the day before experiment (day 0), the day of injections (the 1st day), and then on the 2nd, 6th, and 29th day. The effects of intoxication/treatments on the rotarod test were statistically analyzed by ANOVA. The significance level was set at $p < 0.05$.

3. RESULTS AND DISCUSSION

3.1. Synthesis of Nanoreactor Envelope Polymers. Synthesis of desired polymer mPEG−PPS−mPEG (**6**) was carried out according to Scheme 1, starting from mPEG-750 by the one pot polymerization procedure as described by Napoli et al.,[51] with optimization of the first synthesis step. To avoid using a large amounts of sorbent Sephadex G-25 and very laborious reprecipitation from large amounts of diethyl ether, not allowing to obtain a product of sufficient purity, mPEGTs-750 was prepared by a method,[49] using toluene as the solvent and Et_3N as the base.

The PEG−PPS *block* copolymers are described as the hydrophilic fraction of PEG (f_{PEG}) because this relative *block* composition in general determines the thermodynamically favored morphology in water solutions. f_{PEG} is calculated as $M_w(PEG)/M_w(PEG) + M_w(PPS)$.[54] A clear dependence of PEG−PPS *block* copolymer aggregate morphology on hydrophilic fraction (f_{PEG}) was found[55] for micelles,[37,42] short wormlike micelles,[55] and polymersomes.[56,57] It was shown by Velluto[58] that PEG−PPS can self-assemble in aqueous solution into vesicles, wormlike micelles, and spherical micelles, as the f_{PEG} value ranges from 0.20 to 0.30, from 0.30 to 0.42, and from 0.42 to 0.75, respectively. The optimal hydrophilic fraction f_{PEG} of the total molecular weight for the polymersome formation is equal to or less than 30%. Therefore, in the present work, *block* copolymers were synthesized using amounts of propylene sulfide to give f_{PEG} values about 0.2−0.3. Calculation of the PEG/PPS ratio by comparing the integral intensity of PPS methyl group protons to that of methoxy group protons of mPEG from ^1H NMR (Supporting Information, Figure S3) gave the PEG−PPS ratio as depicted in Scheme 1 and f_{PEG} values of 0.23.

3.2. Building of Polymersomes and Enzyme Encapsulation. The thin-film hydration method is one of the conventional preparation method of polymersomes for encapsulation of biomolecules such us proteins,[31,59] adjuvants, and protein antigens.[57,60] The direct hydration method[54] and multi-impingement flash nanoprecipitation[61−63] are also suitable to encapsulate biomolecules and hydrophilic drugs into PEG−PPS polymersomes. However, all methods mentioned above require additional processing steps, primarily extrusion through nanoporous membranes, homogenization process, freeze−thaw cycles, and the use of organic solvent(s).

https://doi.org/10.1021/acsami.2c03210
ACS Appl. Mater. Interfaces XXXX, XXX, XXX−XXX

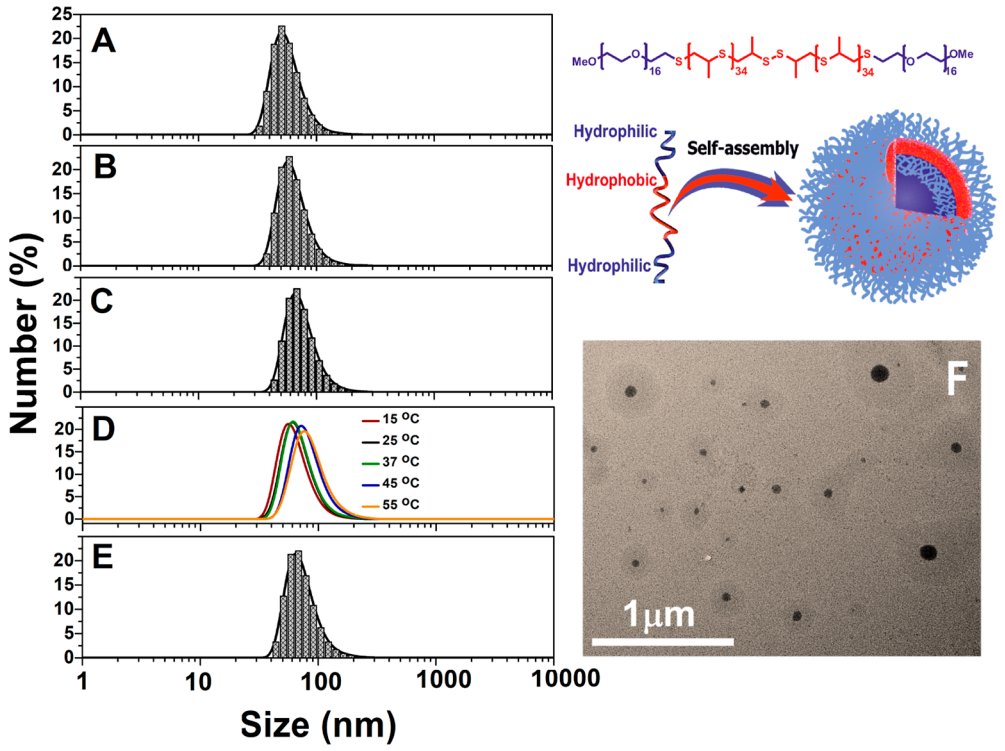

Figure 3. Number size distribution (A–E) and TEM imaging (F) for PEG_{16}–PPS_{68}–PEG_{16} polymersomes, and copolymer concentrations 0.1 (A), 0.2 (B), 0.5 (C), 1 (D), 2% (E) (wt/wt), 25 °C.

Table 1. Enzyme (PTE)- and pNp-Loaded-Polymersomes Characteristics, 10 mM Tris-Buffer, pH = 7.4, 25 °C

				size (nm)						
no	$C_{PEG-PPS-PEG}$, (% wt/wt)	drug-loaded concentration (mM)		int	num	Z-average (nm)	PDI	Z (mV)	EE, (%)	LC, (%)
1	1	PTE	0.02	190 ± 23	79 ± 16	175 ± 1	0.18 ± 0.01	−19 ± 1	83.9 ± 4.35	12.08 ± 0.63
1[a]	1	PTE	0.02	190 ± 20	79 ± 16	180 ± 0.5	0.17 ± 0.01	−11 ± 1		
2	0.5	pNp	7.2	122 ± 18	68 ± 16	117 ± 1	0.15 ± 0.01	−17.3 ± 1	97 ± 2	19.4 ± 0.2
3	1	pNp	7.2	122 ± 20	79 ± 18	119 ± 1	0.08 ± 0.01	−15 ± 1	96 ± 1	9.6 ± 0.1
3[a]	1	pNp	7.2	106 ± 20	68 ± 17	101 ± 1	0.07 ± 0.01	−19.6 ± 1	96 ± 0.5	9.6 ± 0.1
4	2	pNp	7.2	142 ± 62	67 ± 12	134 ± 1	0.23 ± 0.01		98 ± 0.5	4.9 ± 0.03
4[a]	2	pNp	7.2	122 ± 13	58 ± 13	121 ± 1	0.07 ± 0.01	−15.1 ± 0.1	98 ± 0.5	4.9 ± 0.03
5	3	pNp	7.2	106 ± 8	51 ± 13	136 ± 1	0.35 ± 0.01	−17.6 ± 0.1	98 ± 1	3.3 ± 0.03

[a]6 month storage.

The protocol we developed for making PTE-loaded nanoreactors is a simple thin-film hydration method, excluding any additional processing steps as mentioned above. The method we used first avoids the denaturing effect of organic solvents on PTE and second prevents shear stress-induced unfolding of PTE.

The activity of the enzyme was controlled after each step, using POX as the substrate at pH 7.4 and 25 °C. The bimolecular constant $k_{cat}/K_m = 1.02 \pm 0.25 \times 10^5\ M^{-1}\ s^{-1}$ was close to the reported value.[64] Other catalytic parameters we determined are $K_m = 719 \pm 118\ \mu M$ and $k_{cat} = 73.5 \pm 1.7\ s^{-1}$. The enzyme was stable all along the preparation process and upon storage. At 37 °C, in the same buffer, catalytic parameters were similar with $k_{cat}/K_m = 1.07 \pm 0.11 \times 10^5\ M^{-1}\ s^{-1}$. This gives for the mutant enzyme a Q_{10} value close to 1. This value, much lower than for mesophilic enzymes (Q_{10} ranging between 2 and 3), is in agreement with reported values for thermophilic and hyperthermophilic enzymes.[65] Therefore, the effect of temperature in catalytic behavior of the enzyme is the same at 25 and 37 °C.

All characteristics and shape of empty PEG_{16}-PPS_{68}-PEG_{16} polymersomes (without PTE) are presented in Figure 3 and in the Supporting Information file in Table S1 and Figure S11 (intensity size distribution). Several concentrations of *block* copolymers from 0.1 to 3% (wt/wt) were used for the preparation of polymersomes. Hereinafter, this allowed for investigation of the effect of membrane thickness on permeability of reagents/products (POX/pNp). As seen, the number-weighted distributions (Figure 3A–E) and an intensity-weighted distribution (Figure S11) give close results even with increasing *block* copolymer concentrations and increasing the temperature up to 55 °C (Figure 3D). As we see in Table S1, the Z-average size (Z_{aver}, nm) for PEG_{16}–PPS_{68}–PEG_{16} polymersomes (1% wt/wt) is 113 ± 1 nm and PDI is 0.12 ± 0.01. All polymersome samples are monodisperse, PDI

https://doi.org/10.1021/acsami.2c03210
ACS Appl. Mater. Interfaces XXXX, XXX, XXX−XXX

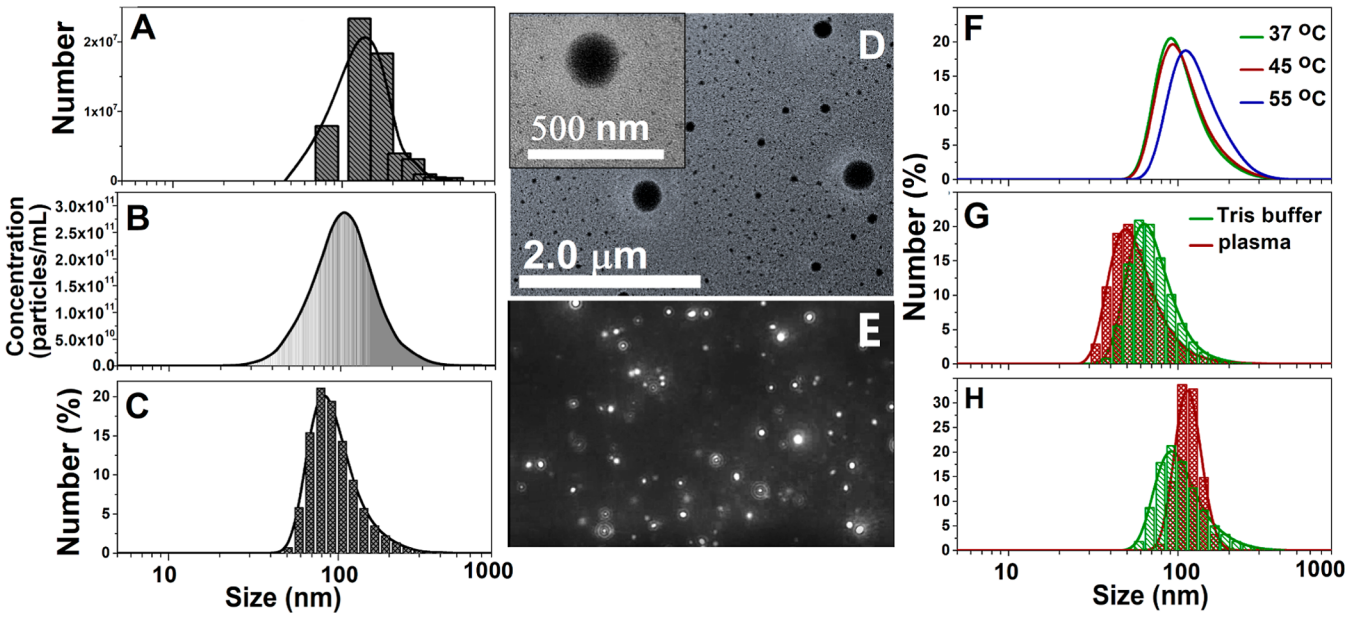

Figure 4. Size distribution as determined by TEM (A), NTA (B), and DLS (C), TEM imaging (D), screenshot of the video from NanoSight LM10 (E) of PTE-loaded nanoreactors at 25 °C and monitoring the stability at different temperatures (F) and *in vitro* conditions in Tris buffer and human plasma within 1 h at 37 °C of PTE-loaded nanoreactors (F,H) and empty nanoreactors (G).

≤ 0.2. The size quality report is presented in the Supporting Information file (Figure S12).

Polymersome size values obtained by TEM (Figure 3F) confirmed DLS data even at the dilution (PEG_{16}–PPS_{68}–PEG_{16}, 20 μg/mL). Spheres of 100–200 nm diameter with a surface covered by a thick "cloud-cap" likely a PEG crown were observed (Figure 3F).

The zeta potential of PEG_{16}–PPS_{68}–PEG_{16} polymersomes varied between −11 and −12 mV with the increasing *block* copolymer concentration (Supporting Information file, Table S1). This negative zeta potential value indicates the overall structural stability of all produced samples.[66] Most likely, the stability of observed particles with a PEG crown for membrane-forming *block* copolymers results from hydrogen bonding. Monitoring of colloidal stability upon storage (at 4 °C) indicates good stability. The size and PDI remained constant (around 100 nm and less than 0.2) during 6 months (Supporting Information file, Table S1).

All characteristics of PTE- and pNp-loaded polymersomes and colloid stability (6 months storage) are presented in Table 1.

The EE and LC for PTE is 84 and 12%, respectively, that is much higher than that for previously reported encapsulated biomacromolecules. It was found[54] that optimization of polymersome preparation techniques is possible to increase the EE of proteins: ovalbumin is 37%, bovine serum albumin is 19%, and bovine γ-globulin is 15%. The EE for the small organic molecule like pNp is very high, increasing from 96 to 98%, depending on the concentration of the *block* copolymer. UV spectra of pNp are presented in the Supporting Information file (Figure S13).

Nanoreactor size was evaluated by three methods: TEM, DLS, and NTA (Figure 4A–C).

The results of three methods are in good agreement with *Z*-average size values: 137 nm (TEM), 175 ± 1 nm (DLS). NTA showed that the mean and mode hydrodynamic diameter of PTE-loaded nanoreactors were 139 ± 3.5 and 106 ± 3.1 nm, respectively (mean ± standard deviation of n = 3 particle batches), indicating that the nanoreactors are within the ∼100 nm size range. PTE-loaded nanoreactors with a spherical shape were observed on the TEM picture (Figure 4D). The screenshot of the video from NanoSight LM10 showing optimal light scatter from PTE-loaded nanoreactors (Figure 4E, multi-media file in Supporting Information). The NTA technique can determine the size distribution as well as the concentration of a sample.[67,68] The NTA method was used to determine the concentration of PTE-loaded nanoreactors (Figure 4B). Taking into account the dilution of the PTE-loaded nanoreactor sample, the determined concentration was 3.21 ± 0.36 × 10^{13} particles/mL. Our calculations for the concentration of PTE inside nanoreactors are based on the limiting assumptions that the geometry and distribution of nanoreactors are spherical and monodisperse. Taking 139 ± 3.5 and 106 ± 3.1 nm as the average diameter of nanoreactors in Tris buffer and EE (%) = 83.9 ± 4.35, the total volumes of nanoreactors/mL are 0.0451 ± 0.005 and 0.02 ± 0.0022 cm^3, respectively, and the concentrations of PTE inside nanoreactors are 0.17 ± 0.0189 and 0.93 ± 0.09 mM, respectively.

PTE-loaded nanoreactors are stable at different increasing temperatures (Figure 4F) and over time (6 months) upon storage at 4 °C (Table 1). Furthermore, they have been verified to maintain the desired colloidal stability both *in vitro* conditions in Tris buffer and in human plasma for 1 h at 37 °C (Figure 4G,H). The size of empty polymersomes slightly decreases, while the size of PTE-loaded polymersomes increases and PDI is also increased achieving 0.3 and 0.6, respectively (Supporting Information file, Table S2). Owing to concentration differences on the both sides of polymeric envelopes: between the encapsulated enzyme inside the nanoreactor and buffer or plasma as outside mediums, volume changes of nanoreactors reflect osmotic effects. Osmotic effects may have important consequences on the catalytic behavior of encapsulated enzymes at high concentration, in changing the reaction order due to enzyme dilution.[69] Taking 106 nm as the

https://doi.org/10.1021/acsami.2c03210
ACS Appl. Mater. Interfaces XXXX, XXX, XXX−XXX

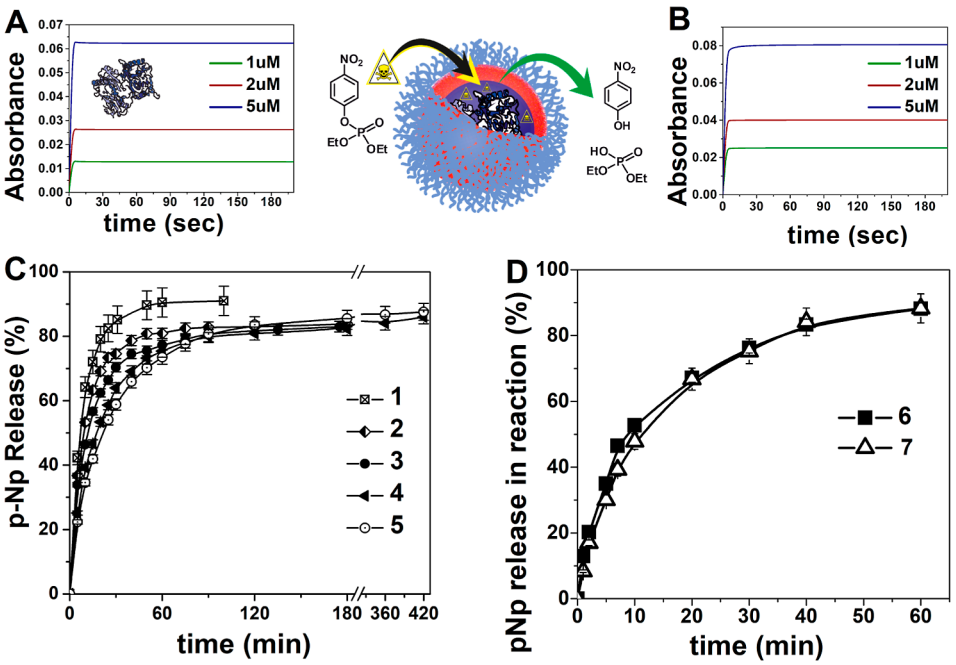

Figure 5. Kinetics of the POX detoxification process by PTE in solution (A) and after encapsulation (B) at λ = 400 nm, 25 °C; pNp release from the polymersome nanoreactor (C,D), where 1-control (without polymersomes), $C_{PEG-PPS-PEG}$ (wt/wt) = 0.5% (2), 1% (3), 2% (4), 3% (5) and after the neutralization of POX by PTE (6) and PTE-loaded polymersomes (7), with C_{pNp} = 5 μM in dialysis bag, C_{POX} = 5 μM, C_{PTE} = 1 μM, 10 mM Tris buffer pH 7.4, 37 °C.

average diameter of nanoreactors in Tris buffer, the volume of nanoreactors containing 0.93 mM PTE increased (33%) in human plasma (the average protein concentration in human plasma is 1 mM) due to entrance of water molecules. However, it leads only to a moderate decrease in PTE concentration inside nanoreactors. This would not affect the reaction order even in the most severe cases of OP poisoning, where the toxicant concentration in plasma may reach 5 μM.

3.3. Membrane Permeability to Substrates/Products and *in Vitro* Simulation of Nanoreactor Activity. The control of polymersome membrane parameters, in particular, permeability to analytes (gases, ions, organic molecules, and macromolecules) is a serious issue. Some principles for designing methods of quantifying membrane permeability [fluorescence spectroscopy, osmotic swelling, and pulsed-field gradient nuclear magnetic resonance (NMR) spectroscopy] and passage of molecules were proposed.[70] As a rule, membranes of catalytic nanoreactors must have a selective permeability to ensure enzyme retention, while simultaneously substrate and reaction products must diffuse freely through the membrane according to the second Fick's low.[24] Toxic substrate (POX) permeates into PTE-loaded polymersomes, where it is hydrolyzed into harmless products (pNp and diethylphosphoric acid). Reacting encapsulated PTE creates a concentration gradient of POX inside the nanoreactor core (Figure 5).

PTE activity against POX as the substrate in solution (Figure 5A) and encapsulated in the nanoreactor (Figure 5B): taking into account that detoxification processes of toxic molecules have to be fast, the concentration of the nano-encapsulated enzyme, [*E*], has to be as high as possible. Reaction of *E* with POX leads to the release of diethylphosphate and pNp. The hydrolysis reaction kinetics was monitored by spectrophotometry from the absorbance hyperbolic increase at 400 nm as a function of time. *In vitro* simulation of enzyme-catalyzed POX inactivation was completed in less than 10 s with either free (Figure 5A) or PTE-loaded nanoreactor (Figure 5B) due to the combination of high enzyme concentration and high bimolecular reaction rate constant.

The dialysis bag method was used to analyze the polymersome permeability for the reaction product pNp (Figure 5C,D). pNp-loaded polymersomes with a high EE about 96−98% (at different concentrations of *block* copolymers) did not show any alteration in properties during at least 6 months (Table 1). As seen in Figure 5C, there is a slowdown release of pNp from polymersomes as the *block* copolymer concentration increased from 0.5% (5 mg/mL) to 3% (30 mg/mL) (curves 2−5) in comparison with the control (curve 1). In the dialysis bag, complete pNp release occurs in about 4 h. Then, the dialysis method was used to control the release of reaction product pNp when the reaction proceeds with free PTE and PTE loaded in nanoreactors. UV spectra of pNp are presented in the Supporting Information file (Figure S14). As seen, the nontoxic product pNp is released at the same rate both in free enzyme solution and PTE-loaded polymersomes.

The concentration of PTE inside polymersomes was in the range of 0.17 ± 0.0189 and 0.93 ± 0.09 mM. Under such conditions, even in the most severe case of poisoning, reactions in nanoreactors circulating in the bloodstream would be performed under second-order conditions, [*E*] ≥ [POX].

3.4. LD_{50}-Shifts with *i.p.* or *s.c* POX Challenge. Initial POX LD_{50} determination and LD_{50} shift of POX caused by pre- and post-exposure treatment on mice were performed, as described in Section 5. POX administration caused animal prostration, labored breathing, tremor, and death due to respiratory failure. POX *i.p.* and *s.c.* injections in control groups provided LD_{50} = 1.2 and 1.38 mg/kg, respectively. Dose-lethal response curves following POX administration are presented in the Supporting Information file (Figure S15) for *i.p* and in

https://doi.org/10.1021/acsami.2c03210
ACS Appl. Mater. Interfaces XXXX, XXX, XXX−XXX

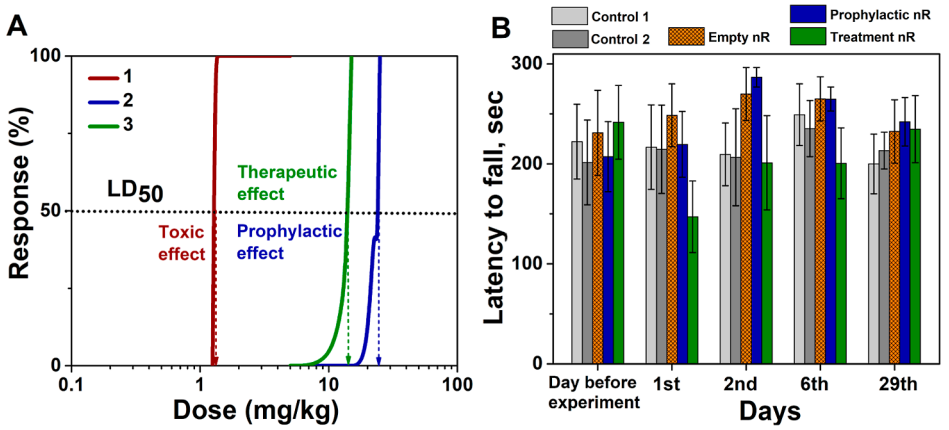

Figure 6. Results of POX-challenged animals pre-treated or post-exposure treated by PTE-containing nanoreactors: (A) LD_{50}-shifts for acute toxicity of POX *s.c.*: 1, nontreated (control) animals; 2, animals under prophylaxis; 3, post-exposure treated animals; (B) rotarod test for mice, latency time to fall: day before POX challenge, the 1st day of experiment, 2nd, 6th, and 29th day after challenge.

f6

Figure 6A and for *s.c.* administrations. Tables S3 and S4 in Supporting Information file shows the number of animals for each dose to clarify the choice of the number of animals.

Prophylactic nanoreactor injection significantly shifted POX toxicity toward high toxic doses (LD_{50} *i.p.* = 8.7 mg/kg and LD_{50} *s.c.* = 23.06 mg/kg). In post-exposure treatment, enzyme nanoreactor administration was less effective for both ways of intoxication but still provided a high LD_{50} shift: LD_{50} *i.p.* = 4.1 mg/kg and LD_{50} *s.c.* = 13.64 mg/kg.

The intrananoreactor enzyme concentration determined from NTA measurements was 0.93 mM. Although the molar ratio [*E*]/[POX] in nanoreactors, when POX reaches its maximum concentration in blood after *i.p.* injection, was not accessible experimentally, a rough estimate of the maximum POX concentration in mouse blood (2 mL) can be calculated on the basis of LD_{50} shifts POX concentrations from prophylaxis and post-exposure treatment experiments. These estimated [POX] are 0.32 and 0.15 mM, respectively, values much lower than the encapsulated enzyme concentration. Thus, it can reasonably be stated that the neutralization reaction fulfill the second-order conditions, that is, [*E*] > [POX]. Moreover, because the enzyme displays a high bimolecular rate constant against POX ($1.02 \pm 0.25 \times 10^5$ M^{-1} s^{-1} at pH 7.4, present result), the hyperbolic time-dependent inactivation of POX under second-order reaction leads to a rapid decrease in POX toxic concentration in blood. The remaining POX molecules present in the bloodstream and/or further released from depot sites can be inactivated by other endogenous bioscavengers, for example, albumin, plasma butyrylcholinesterase (BChE), and carboxylesterases.

3.5. Rotarod Test. On the day of experiment, after prophylactic treatment (4th group of animals) and post-exposure treatment (5th group of animals) by PTE-loaded nanoreactors, animals were transiently prostrate after POX challenge, but at the same time, they did not fail at the rotarod test (Figure 6B). The latency to fall at rotarod test for mice (n = 6), in seconds is presented in the Supporting Information file (Table S5). Despite mild sedation during the next few hours after POX challenge, animals completely recovered on the second day. ANOVA statistical analysis of the rotarod test showed that there is no significant difference in animal performances at the confidence level of 95% between control and treated groups on the first and subsequent days of the study.

4. CONCLUSIONS

We have successfully prepared a very simple, easy to manufacture, and biocompatible formulation for PTE-loaded nanoreactors. The therapeutic nanoreactor containing an evolved mutant of *Saccharolobus solfataricus* PLL optimized for its PTE properties was found to be very efficient in pre- and post-exposure treatment of mice against POX poisoning. Results showed that *i.v* administration of the nanoreactor-encapsulated PTE mutant (enzyme dose = 1.6 nmoles) is capable of protecting mice against high doses of POX: 7 × LD_{50} POX *i.p.* and 16.6 × LD_{50} POX *s.c.* in pre-treatment and 3.3 × LD_{50} POX *i.p.* and 9.8 × LD_{50} POX *s.c.* in post-exposure treatment. Animals survived without any additional pharmacological pre-treatment. Although no sophisticated quantitative neuromuscular and behavioral tests were performed, post-challenge observation of surviving animals in the following hours and days did not reveal any sign of irreversible brain or muscular damages. In addition, rotarod tests showed that protected or treated animals passed the test, like control groups, after challenge by 0.5 × LD_{50} POX. The rotarod test did not reveal alteration in performance up to 6 days, after POX challenge. An ultimate rotarod test, 28 days after the challenge, did not show any deterioration in performances. However, further refined behavioral, physiological, and cytological studies are underway to investigate possible central and neuromuscular sequelae. Moreover, we still do not know the fate of nanoreactors in the blood stream. Pharmacokinetics and immunological investigations are underway to answer this issue.

The present achievement is the first step toward the creation of more complex nanoreactors, containing several enzymes and adjuncts aimed at broadening the spectrum of degradable OPs in very short times without adverse effects.

■ ASSOCIATED CONTENT

Supporting Information

The Supporting Information is available free of charge at https://pubs.acs.org/doi/10.1021/acsami.2c03210.

Rational for choosing PEG and PPS and interests of these polymers for making nanoreactor envelopes, including specific SI references, ^{1}H NMR spectra of synthesized compounds, ^{13}C NMR spectra of the mPEG−PPS−mPEG copolymer, IR spectra of mPEG

https://doi.org/10.1021/acsami.2c03210
ACS Appl. Mater. Interfaces XXXX, XXX, XXX−XXX

derivatives, IR spectra of the mPEG−PPS−mPEG copolymer, UV absorbance spectra and calibration curve of β-lactoglobulin pNp in Tris buffer, transmittance of polymersomes under centrifugation conditions versus time, particle size distribution using the intensity parameter for polymersomes, screenshot of particle size distribution for polymersomes, UV absorbance spectra of pNp for EE of polymersomes, UV absorbance spectra of pNp after neutralization of POX by PTE and PTE-loaded polymersomes, dose-lethal response curve following POX administration (*i.p.*) in control group prophylactic and post-exposure treatments by PTE-loaded nanoreactors, empty polymersome characteristics, *in vitro* stability of empty and PTE-loaded polymersome characteristics, prophylaxis and post-exposure treatment of POX *i.p.* acute toxicity by *i.v.* administration of PTE-loaded nanoreactors in mice, prophylaxis and post-exposure treatment of POX *s.c.* acute toxicity by *i.v.* administration of PTE-loaded nanoreactors in mice, latency to fall at the rotarod test for mice ($n = 6$) in seconds (mean ± SEM), and brief description (PDF)

AUTHOR INFORMATION

Corresponding Author

Patrick Masson − *Biochemical Neuropharmacology Laboratory, Kazan Federal University, Kazan 420111, Russian Federation*; Email: pym.masson@free.fr

Authors

Tatiana Pashirova − *Arbuzov Institute of Organic and Physical Chemistry, FRC Kazan Scientific Center, Russian Academy of Sciences, Kazan 420088, Russian Federation*; orcid.org/0000-0002-2001-1570

Zukhra Shaihutdinova − *Arbuzov Institute of Organic and Physical Chemistry, FRC Kazan Scientific Center, Russian Academy of Sciences, Kazan 420088, Russian Federation; Biochemical Neuropharmacology Laboratory, Kazan Federal University, Kazan 420111, Russian Federation*

Milana Mansurova − *Biochemical Neuropharmacology Laboratory, Kazan Federal University, Kazan 420111, Russian Federation*

Renata Kazakova − *Biochemical Neuropharmacology Laboratory, Kazan Federal University, Kazan 420111, Russian Federation*

Dinara Shambazova − *Biochemical Neuropharmacology Laboratory, Kazan Federal University, Kazan 420111, Russian Federation*

Andrei Bogdanov − *Arbuzov Institute of Organic and Physical Chemistry, FRC Kazan Scientific Center, Russian Academy of Sciences, Kazan 420088, Russian Federation*

Dmitry Tatarinov − *Arbuzov Institute of Organic and Physical Chemistry, FRC Kazan Scientific Center, Russian Academy of Sciences, Kazan 420088, Russian Federation*; orcid.org/0000-0002-9960-7499

David Daudé − *Gene&GreenTK, Marseille 13005, France*

Pauline Jacquet − *Gene&GreenTK, Marseille 13005, France*

Eric Chabrière − *Gene&GreenTK, Marseille 13005, France; Aix Marseille University, IRD, APHM, MEPHI, IHU-Méditerranée Infection, Marseille 13005, France*

Complete contact information is available at: https://pubs.acs.org/10.1021/acsami.2c03210

Author Contributions

The manuscript was written through contributions of all authors. All authors have given approval to the final version of the manuscript. Z.S., D.S., and T.P. built nanoreactors and performed biochemical and physicochemical measurements; M.M. and R.K. performed animal studies; A.B. and D.T. synthesized polymeric envelopes of nanoreactors; D.D., P.J., and E.C. produced the mutant of SsoPOX phosphotriesterase; and T.P. and P.M. wrote the manuscript.

Funding

This study was funded by Russian Science Foundation grant # 20-14-00155 to P.M., T.P., and M.M.

Notes

The authors declare the following competing financial interest(s): E.C. and D.D. have filed the patent FR3068989. P.J., D.D., and E.C. report receiving personal fees from Gene&GreenTK during the study. E.C. and D.D. are shareholders in Gene&GreenTK. D.D. is CEO of Gene&GreenTK. E.C. and D.D. have filed the patent FR3068989. P.J., D.D., and E.C. report receiving personal fees from Gene&GreenTK during the study. E.C. and D.D. are shareholders in Gene&GreenTK. D.D. is CEO of Gene&GreenTK.

ACKNOWLEDGMENTS

The authors are grateful to Vladimir G. Evtjugin (Interdisciplinary Center of Analytical Microscopy, Kazan Federal University) for study of TEM and research and assistance. The authors are also indebted to Marianna P. Kutyreva and Arthur A. Khannanov (Inorganic Chemistry Department of the Chemistry Institute of Kazan Federal University) for providing access to NanoSight LM10 (Malvern Panalytical, Worcestershire, UK).

ABBREVIATIONS

AChE, acetylcholinesterase
BChE, butyrylcholinesterase
$CDCl_3$, deuteriochloroform
DCM, dichloromethane
DLS, dynamic light scattering
DMF, *N*,*N*-dimethylformamide
NTA, nanoparticle tracking analysis
OP, organophosphorous compound
PDI, polydispersity index
PEG, polyethylene glycol
PLL, phosphotriesterase-like lactonase
pNp, *p*-nitrophenol
POX, ethyl-paraoxon
PPS, polypropylene sulfide
PTE, phosphotriesterase
TEM, transmission electron microscopy
THF, tetrahydrofuran

REFERENCES

(1) Eddleston, M. Novel Clinical Toxicology and Pharmacology of Organophosphorus Insecticide Self-Poisoning. *Annu. Rev. Pharmacol. Toxicol.* **2019**, *59*, 341−360.

(2) Aroniadou-Anderjaska, V.; Apland, J. P.; Figueiredo, T. H.; De Araujo Furtado, M.; Braga, M. F. Acetylcholinesterase Inhibitors (Nerve Agents) as Weapons of Mass Destruction: History, Mechanisms of Action, and Medical Countermeasures. *Neuropharmacology* **2020**, *181*, 108298.

https://doi.org/10.1021/acsami.2c03210
ACS Appl. Mater. Interfaces XXXX, XXX, XXX−XXX

(3) Colovic, M. B.; Krstic, D. Z.; Lazarevic-Pasti, T. D.; Bondzic, A. M.; Vasic, V. M. Acetylcholinesterase Inhibitors: Pharmacology and Toxicology. *Curr. Neuropharmacol.* **2013**, *11*, 315−335.
(4) Masson, P.; Nachon, F. Cholinesterase Reactivators and Bioscavengers for Pre- and Post-Exposure Treatments of Organophosphorus Poisoning. *J. Neurochem.* **2017**, *142*, 26−40.
(5) Xu, F.; Kang, T.; Deng, J.; Liu, J.; Chen, X.; Wang, Y.; Ouyang, L.; Du, T.; Tang, H.; Xu, X.; Chen, S.; Du, Y.; Shi, Y.; Qian, Z.; Wei, Y.; Deng, H.; Gou, M. Functional Nanoparticles Activate a Decellularized Liver Scaffold for Blood Detoxification. *Small* **2016**, *12*, 2067−2076.
(6) Wang, J.; Li, Y.; Huang, J.; Li, W.; Luo, Y.; Sui, X.; Li, J.; Wang, Y.; Yang, J. A Protein Nanocomposite for Ultra-Fast, Efficient and Non-Irritating Skin Decontamination of Nerve Agents. *Nanoscale* **2020**, *12*, 4400−4409.
(7) Chen, Y.; Chen, M.; Zhang, Y.; Lee, J. H.; Escajadillo, T.; Gong, H.; Fang, R. H.; Gao, W.; Nizet, V.; Zhang, L. Broad-Spectrum Neutralization of Pore-Forming Toxins with Human Erythrocyte Membrane-Coated Nanosponges. *Adv. Healthcare Mater.* **2018**, *7*, 1−10.
(8) Liu, Y.; Du, J.; Yan, M.; Lau, M. Y.; Hu, J.; Han, H.; Yang, O. O.; Liang, S.; Wei, W.; Wang, H.; Li, J.; Zhu, X.; Shi, L.; Chen, W.; Ji, C.; Lu, Y. Biomimetic Enzyme Nanocomplexes and Their Use as Antidotes and Preventive Measures for Alcohol Intoxication. *Nat. Nanotechnol.* **2013**, *8*, 187−192.
(9) Tian, M.; Xing, R.; Guan, J.; Yang, B.; Zhao, X.; Yang, J.; Zhan, C.; Zhang, S. A Nanoantidote Alleviates Glioblastoma Chemotoxicity without Efficacy Compromise. *Nano Lett.* **2021**, *21*, 5158−5166.
(10) Liu, Y.; Li, J.; Lu, Y. Enzyme Therapeutics for Systemic Detoxification. *Adv. Drug Deliv. Rev.* **2015**, *90*, 24−39.
(11) Forster, V.; Leroux, J.-C. Nano-Antidotes for Drug Overdose and Poisoning. *Sci. Transl. Med.* **2015**, *7*, 290ps14.
(12) Rabanel, J.-M.; Delbreil, P.; Banquy, X.; Brambilla, D.; Ramassamy, C. Periphery-Confined Particulate Systems for the Management of Neurodegenerative Diseases and Toxicity: Avoiding the Blood-Brain-Barrier Challenge. *J. Controlled Release* **2020**, *322*, 286−299.
(13) Pashirova, T. N.; Zueva, I. V.; Petrov, K. A.; Babaev, V. M.; Lukashenko, S. S.; Rizvanov, I. K.; Souto, E. B.; Nikolsky, E. E.; Zakharova, L. Y.; Masson, P.; Sinyashin, O. G. Nanoparticle-Delivered 2-PAM for Rat Brain Protection against Paraoxon Central Toxicity. *ACS Appl. Mater. Interfaces* **2017**, *9*, 16922−16932.
(14) Buzyurova, D. N.; Pashirova, T. N.; Zueva, I. V.; Burilova, E. A.; Shaihutdinova, Z. M.; Rizvanov, I. K.; Babaev, V. M.; Petrov, K. A.; Souto, E. B. Surface Modification of Pralidoxime Chloride-Loaded Solid Lipid Nanoparticles for Enhanced Brain Reactivation of Organophosphorus-Inhibited AChE: Pharmacokinetics in Rat. *Toxicology* **2020**, *444*, 152578.
(15) Pashirova, T. N.; Braïki, A.; Zueva, I. V.; Petrov, K. A.; Babaev, V. M.; Burilova, E. A.; Samarkina, D. A.; Rizvanov, I. K.; Souto, E. B.; Jean, L.; Renard, P.-Y.; Masson, P.; Zakharova, L. Y.; Sinyashin, O. G. Combination Delivery of Two Oxime-Loaded Lipid Nanoparticles: Time-Dependent Additive Action for Prolonged Rat Brain Protection. *J. Controlled Release* **2018**, *290*, 102−111.
(16) Pashirova, T. N.; Zueva, I. V.; Petrov, K. A.; Lukashenko, S. S.; Nizameev, I. R.; Kulik, N. V.; Voloshina, A. D.; Almasy, L.; Kadirov, M. K.; Masson, P.; Souto, E. B.; Zakharova, L. Y.; Sinyashin, O. G. Mixed Cationic Liposomes for Brain Delivery of Drugs by the Intranasal Route: The Acetylcholinesterase Reactivator 2-PAM as Encapsulated Drug Model. *Colloids Surf. B Biointerfaces* **2018**, *171*, 358−367.
(17) Bigley, A. N.; Harvey, S. P.; Narindoshvili, T.; Raushel, F. M. Substrate Analogues for the Enzyme-Catalyzed Detoxification of the Organophosphate Nerve Agents—Sarin, Soman, and Cyclosarin. *Biochemistry* **2021**, *60*, 2875−2887.
(18) Jacquet, P. Amélioration d'une Enzyme Hyperthermostable Pour La Dégradation Des Organophosphorés. Ph.D. Thesis, Aix-Marseille University (France), 2017.
(19) Ashani, Y.; Rothschild, N.; Segall, Y.; Levanon, D.; Raveh, L. Prophylaxis against Organophsphate Poisoning by an Enzyme Hydrolysing Organophosphorus Compounds in Mice. *Life Sci.* **1991**, *49*, 367−374.
(20) Kalistekorhonen, E.; Ylitalo, P.; Hanninen, O.; Raushel, F. M. Phosphotriesterase Decreases Paraoxon Toxicity in Mice. *Toxicol. Appl. Pharmacol.* **1993**, *121*, 275−278.
(21) Broomfield, C. A. A Purified Recombinant Organophosphorus Acid Anhydrase Protects Mice against Soman. *Chem. Biol. Interact.* **1993**, *87*, 279−84.
(22) Petrikovics, I.; Papahadjopoulos, D.; Hong, K.; Cheng, T. C.; Baskin, S. I.; Jiang, J.; Jaszberenyi, J. C.; Logue, B. A.; Szilasi, M.; McGuinn, W. D.; Way, J. L. Comparing Therapeutic and Prophylactic Protection against the Lethal Effect of Paraoxon. *Toxicol. Sci.* **2004**, *77*, 258−262.
(23) Zhang, P.; Liu, E. J.; Tsao, C.; Kasten, S. A.; Boeri, M. V.; Dao, T. L.; DeBus, S. J.; Cadieux, C. L.; Baker, C. A.; Otto, T. C.; Cerasoli, D. M.; Chen, Y.; Jain, P.; Sun, F.; Li, W.; Hung, H.-C.; Yuan, Z.; Ma, J.; Bigley, A. N.; Raushel, F. M.; Jiang, S. Nanoscavenger Provides Long-Term Prophylactic Protection against Nerve Agents in Rodents. *Sci. Transl. Med.* **2019**, *11*, No. eaau7091.
(24) Pashirova, T. N.; Bogdanov, A.; Masson, P. Therapeutic Nanoreactors for Detoxification of Xenobiotics: Concepts, Challenges and Biotechnological Trends with Special Emphasis to Organophosphate Bioscavenging. *Chem. Biol. Interact.* **2021**, *346*, 109577.
(25) Discher, B. M.; Won, Y.-Y.; Ege, D. S.; Lee, J. C.-M.; Bates, F. S.; Discher, D. E.; Hammer, D. A. Polymersomes: Tough Vesicles Made from Diblock Copolymers. *Science* **1999**, *284*, 1143−1146.
(26) Nardin, C.; Hirt, T.; Leukel, J.; Meier, W. Polymerized ABA Triblock Copolymer Vesicles. *Langmuir* **2000**, *16*, 1035−1041.
(27) Napoli, A.; Tirelli, N.; Wehrli, E.; Hubbell, J. A. Lyotropic Behavior in Water of Amphiphilic ABA Triblock Copolymers Based on Poly(Propylene Sulfide) and Poly(Ethylene Glycol). *Langmuir* **2002**, *18*, 8324−8329.
(28) Matoori, S.; Leroux, J.-C. Twenty-Five Years of Polymersomes: Lost in Translation? *Mater. Horiz.* **2020**, *7*, 1297−1309.
(29) Apolinário, A. C.; Hauschke, L.; Nunes, J. R.; Lopes, L. B. Lipid Nanovesicles for Biomedical Applications: 'What Is in a Name'? *Prog. Lipid Res.* **2021**, *82*, 101096.
(30) Discher, D. E.; Eisenberg, A. Polymer Vesicles. *Science* **2002**, *297*, 967−973.
(31) Lee, J. C.-M.; Bermudez, H.; Discher, B. M.; Sheehan, M. A.; Won, Y.-Y.; Bates, F. S.; Discher, D. E. Preparation, Stability, and in Vitro Performance of Vesicles Made with Diblock Copolymers. *Biotechnol. Bioeng.* **2001**, *73*, 135−145.
(32) Iqbal, S.; Blenner, M.; Alexander-Bryant, A.; Larsen, J. Polymersomes for Therapeutic Delivery of Protein and Nucleic Acid Macromolecules: From Design to Therapeutic Applications. *Biomacromolecules* **2020**, *21*, 1327−1350.
(33) Mertz, M.; Castiglione, K. Increased Protein Encapsulation in Polymersomes with Hydrophobic Membrane Anchoring Peptides in a Scalable Process. *Int. J. Mol. Sci.* **2021**, *22*, 7134.
(34) Pachioni-Vasconcelos, J. D. A.; Lopes, A. M.; Apolinário, A. C.; Valenzuela-Oses, J. K.; Costa, J. S. R.; Nascimento, L. D. O.; Pessoa, A.; Barbosa, L. R. S.; Rangel-Yagui, C. D. O. Nanostructures for Protein Drug Delivery. *Biomater. Sci.* **2016**, *4*, 205−218.
(35) Zhang, C.; Yan, L.; Wang, X.; Zhu, S.; Chen, C.; Gu, Z.; Zhao, Y. Progress, Challenges, and Future of Nanomedicine. *Nano Today* **2020**, *35*, 101008.
(36) Monteiro, P. F.; Travanut, A.; Conte, C.; Alexander, C. Reduction-responsive Polymers for Drug Delivery in Cancer Therapy—Is There Anything New to Discover? *Wiley Interdiscip. Rev.: Nanomed. Nanobiotechnol.* **2021**, *13*, 1−16.
(37) Stack, T.; Vahabikashi, A.; Johnson, M.; Scott, E. Modulation of Schlemm's Canal Endothelial Cell Stiffness via Latrunculin Loaded Block Copolymer Micelles. *J. Biomed. Mater. Res.* **2018**, *106*, 1771−1779.
(38) Geven, M.; d'Arcy, R.; Turhan, Z. Y.; El-Mohtadi, F.; Alshamsan, A.; Tirelli, N. Sulfur-Based Oxidation-Responsive

https://doi.org/10.1021/acsami.2c03210
ACS Appl. Mater. Interfaces XXXX, XXX, XXX−XXX

Polymers. Chemistry, (Chemically Selective) Responsiveness and Biomedical Applications. *Eur. Polym. J.* **2021**, *149*, 110387.
(39) Karabin, N. B.; Allen, S.; Kwon, H.-K.; Bobbala, S.; Firlar, E.; Shokuhfar, T.; Shull, K. R.; Scott, E. A. Sustained Micellar Delivery via Inducible Transitions in Nanostructure Morphology. *Nat. Commun.* **2018**, *9*, 624.
(40) El Mohtadi, F.; d'Arcy, R.; Yang, X.; Turhan, Z. Y.; Alshamsan, A.; Tirelli, N. Main Chain Polysulfoxides as Active 'Stealth' Polymers with Additional Antioxidant and Anti-Inflammatory Behaviour. *Int. J. Mol. Sci.* **2019**, *20* (). https://doi.org/ DOI: 10.3390/ijms20184583.
(41) Zhu, S.; Li, S.; Escuin-Ordinas, H.; Dimatteo, R.; Xi, W.; Ribas, A.; Segura, T. Accelerated Wound Healing by Injectable Star Poly(Ethylene Glycol)-b-Poly(Propylene Sulfide) Scaffolds Loaded with Poorly Water-Soluble Drugs. *J. Controlled Release* **2018**, *282*, 156−165.
(42) Velluto, D.; Bojadzic, D.; De Toni, T.; Buchwald, P.; Tomei, A. A. Drug-Integrating Amphiphilic Nanomaterial Assemblies: 1. Spatiotemporal Control of Cyclosporine Delivery and Activity Using Nanomicelles and Nanofibrils. *J. Controlled Release* **2021**, *329*, 955−970.
(43) Allen, S. D.; Liu, Y.-G.; Bobbala, S.; Cai, L.; Hecker, P. I.; Temel, R.; Scott, E. A. Polymersomes Scalably Fabricated via Flash Nanoprecipitation Are Non-Toxic in Non-Human Primates and Associate with Leukocytes in the Spleen and Kidney Following Intravenous Administration. *Nano Res.* **2018**, *11*, 5689−5703.
(44) Bobbala, S.; Vincent, M. P.; Scott, E. A. Just Add Water: Hydratable, Morphologically Diverse Nanocarrier Powders for Targeted Delivery. *Nanoscale* **2021**, *13*, 11349−11359.
(45) Amitai, G.; Moorad, D.; Adani, R.; Doctor, B. P. Inhibition of Acetylcholinesterase and Butyrylcholinesterase by Chlorpyrifos-Oxon. *Biochem. Pharmacol.* **1998**, *56*, 293−299.
(46) Poirier, L.; Pinault, L.; Armstrong, N.; Ghigo, E.; Daudé, D.; Chabrière, E. Evaluation of a Robust Engineered Enzyme towards Organophosphorus Insecticide Bioremediation Using Planarians as Biosensors. *Chem. Biol. Interact.* **2019**, *306*, 96−103.
(47) Rémy, B.; Plener, L.; Poirier, L.; Elias, M.; Daudé, D.; Chabrière, E. Harnessing Hyperthermostable Lactonase from Sulfolobus Solfataricus for Biotechnological Applications. *Sci. Rep.* **2016**, *6*, 37780.
(48) Jacquet, P.; Hiblot, J.; Daudé, D.; Bergonzi, C.; Gotthard, G.; Armstrong, N.; Chabrière, E.; Elias, M. Rational Engineering of a Native Hyperthermostable Lactonase into a Broad Spectrum Phosphotriesterase. *Sci. Rep.* **2017**, *7*, 16745.
(49) Davis, F.; Van Es, T.; Palczuk, N. Non-Immunogenic Polypeptides. U.S. Patent 4,179,337 A, 1979.
(50) Mahou, R.; Wandrey, C. Versatile Route to Synthesize Heterobifunctional Poly(Ethylene Glycol) of Variable Functionality for Subsequent Pegylation. *Polym.* **2012**, *4*, 561−589.
(51) Napoli, A.; Tirelli, N.; Kilcher, G.; Hubbell, A. New Synthetic Methodologies for Amphiphilic Multiblock Copolymers of Ethylene Glycol and Propylene Sulfide. *Macromolecules* **2001**, *34*, 8913−8917.
(52) Brooks, S. P.; Trueman, R. C.; Dunnett, S. B. Assessment of Motor Coordination and Balance in Mice Using the Rotarod, Elevated Bridge, and Footprint Tests. *Current Protocols in Mouse Biology*; John Wiley & Sons, Inc.: Hoboken, NJ, USA, 2012; Vol. 2, pp 37−53.
(53) Lee, B.; Park, S. M.; Jeong, S.; Kim, K.; Jeung, E.-B. Combined Exposure to Diazinon and Nicotine Exerts a Synergistic Adverse Effect In Vitro and Disrupts Brain Development and Behaviors In Vivo. *Int. J. Mol. Sci.* **2021**, *22*, 7742.
(54) O'Neil, C. P.; Suzuki, T.; Demurtas, D.; Finka, A.; Hubbell, J. A. A Novel Method for the Encapsulation of Biomolecules into Polymersomes via Direct Hydration. *Langmuir* **2009**, *25*, 9025−9029.
(55) Cerritelli, S.; Fontana, A.; Velluto, D.; Adrian, M.; Dubochet, J.; De Maria, P.; Hubbell, J. A. Thermodynamic and Kinetic Effects in the Aggregation Behavior of a Poly(Ethylene Glycol- b- Propylene Sulfide- b -Ethylene Glycol) ABA Triblock Copolymer. *Macromolecules* **2005**, *38*, 7845−7851.
(56) Cerritelli, S.; Velluto, D.; Hubbell, J. A. PEG-SS-PPS: Reduction-Sensitive Disulfide Block Copolymer Vesicles for Intracellular Drug Delivery. *Biomacromolecules* **2007**, *8*, 1966−1972.
(57) Scott, E. A.; Stano, A.; Gillard, M.; Maio-Liu, A. C.; Swartz, M. A.; Hubbell, J. A. Dendritic Cell Activation and T Cell Priming with Adjuvant- and Antigen-Loaded Oxidation-Sensitive Polymersomes. *Biomaterials* **2012**, *33*, 6211−6219.
(58) Velluto, D.; Demurtas, D.; Hubbell, J. A. PEG- b -PPS Diblock Copolymer Aggregates for Hydrophobic Drug Solubilization and Release: Cyclosporin A as an Example. *Mol. Pharm.* **2008**, *5*, 632−642.
(59) Napoli, A.; Boerakker, M. J.; Tirelli, N.; Nolte, R. J. M.; Sommerdijk, N. A. J. M.; Hubbell, J. A. Glucose-Oxidase Based Self-Destructing Polymeric Vesicles. *Langmuir* **2004**, *20*, 3487−3491.
(60) Stano, A.; Scott, E. A.; Dane, K. Y.; Swartz, M. A.; Hubbell, J. A. Tunable T Cell Immunity towards a Protein Antigen Using Polymersomes vs. Solid-Core Nanoparticles. *Biomaterials* **2013**, *34*, 4339−4346.
(61) Allen, S.; Osorio, O.; Liu, Y.-G.; Scott, E. Facile Assembly and Loading of Theranostic Polymersomes via Multi-Impingement Flash Nanoprecipitation. *J. Controlled Release* **2017**, *262*, 91−103.
(62) Allen, S. D.; Bobbala, S.; Karabin, N. B.; Modak, M.; Scott, E. A. Benchmarking Bicontinuous Nanospheres against Polymersomes for in Vivo Biodistribution and Dual Intracellular Delivery of Lipophilic and Water-Soluble Payloads. *ACS Appl. Mater. Interfaces* **2018**, *10*, 33857−33866.
(63) Vincent, M. P.; Karabin, N. B.; Allen, S. D.; Bobbala, S.; Frey, M. A.; Yi, S.; Yang, Y.; Scott, E. A. The Combination of Morphology and Surface Chemistry Defines the Immunological Identity of Nanocarriers in Human Blood. *Adv. Ther.* **2021**, *4*, 2100062.
(64) Poirier, L.; Jacquet, P.; Plener, L.; Masson, P.; Daudé, D.; Chabrière, E. Organophosphorus Poisoning in Animals and Enzymatic Antidotes. *Environ. Sci. Pollut. Res.* **2021**, *28*, 25081−25106.
(65) Elias, M.; Wieczorek, G.; Rosenne, S.; Tawfik, D. S. The Universality of Enzymatic Rate−Temperature Dependency. *Trends Biochem. Sci.* **2014**, *39*, 1−7.
(66) Frey, M.; Vincent, M.; Bobbala, S.; Burt, R.; Scott, E. Mapping the Supramolecular Assembly Space of Poly(Sarcosine)- b -Poly-(Propylene Sulfide) Using a Combinatorial Copolymer Library. *Chem. Commun.* **2020**, *56*, 6644−6647.
(67) Hole, P.; Sillence, K.; Hannell, C.; Maguire, C. M.; Roesslein, M.; Suarez, G.; Capracotta, S.; Magdolenova, Z.; Horev-Azaria, L.; Dybowska, A.; Cooke, L.; Haase, A.; Contal, S.; Manø, S.; Vennemann, A.; Sauvain, J.-J.; Staunton, K. C.; Anguissola, S.; Luch, A.; Dusinska, M.; Korenstein, R.; Gutleb, A. C.; Wiemann, M.; Prina-Mello, A.; Riediker, M.; Wick, P. Interlaboratory Comparison of Size Measurements on Nanoparticles Using Nanoparticle Tracking Analysis (NTA). *J. Nanoparticle Res.* **2013**, *15*, 2101.
(68) Maguire, C. M.; Sillence, K.; Roesslein, M.; Hannell, C.; Suarez, G.; Sauvain, J.-J.; Capracotta, S.; Contal, S.; Cambier, S.; El Yamani, N.; Dusinska, M.; Dybowska, A.; Vennemann, A.; Cooke, L.; Haase, A.; Luch, A.; Wiemann, M.; Gutleb, A.; Korenstein, R.; Riediker, M.; Wick, P.; Hole, P.; Prina-Mello, A. Benchmark of Nanoparticle Tracking Analysis on Measuring Nanoparticle Sizing and Concentration. *J. Micro Nano-Manufacturing* **2017**, *5*, 1−10.
(69) Shajhutdinova, Z.; Pashirova, T.; Masson, P. Kinetic Processes in Enzymatic Nanoreactors for In Vivo Detoxification. *Biomedicines* **2022**, *10*, 784.
(70) Miller, A. J.; Pearce, A. K.; Foster, J. C.; O'Reilly, R. K. Probing and Tuning the Permeability of Polymersomes. *ACS Cent. Sci.* **2021**, *7*, 30−38.

https://doi.org/10.1021/acsami.2c03210
ACS Appl. Mater. Interfaces XXXX, XXX, XXX−XXX